

Quantitative determination of the structural units in phosphorus-selenium glasses by ^{31}P dipolar and magic-angle-spinning NMR spectroscopy

David Lathrop and Hellmut Eckert

Department of Chemistry, University of California, Santa Barbara, Goleta, California 93106

(Received 13 September 1990)

The detailed quantitative speciation of phosphorus and selenium microstructures in phosphorus-selenium glasses is derived from combined ^{31}P spin-echo and magic-angle-spinning NMR experiments. The results illustrate that the structure of these glasses differs from the chemically ordered or clustered structures previously proposed, but are also at variance with a completely random distribution. There is a distinct preference for the formation of P—Se versus P—P and Se—Se bonds, which can be quantified from the present experiments. The site speciation shows no dramatic changes near the composition (40 at. % P) corresponding to the rigidity percolation threshold.

INTRODUCTION

Nonoxide chalcogenide glasses, which are based on the sulfides, selenides, and tellurides of the main group-III–V elements, are a promising class of solid-state materials, with intriguing possibilities for applications as low-frequency waveguides and fibers, amorphous semiconductors, and solid electrolytes.^{1–3} During the last two decades much work has been devoted to the phase diagrams, regions of glass formation, and the physical properties of these systems. Much more recently, driven by the search for guidelines to optimize materials properties, the microscopic structure of these glasses has moved into the focus of attention. At the same time, chalcogenide glasses have become an important testing ground for theories dealing with the driving forces of glass formation in covalent systems.^{4–6} To date, the structural investigation of these systems has relied heavily on diffraction experiments, extended x-ray-absorption fine structure (EXAFS), and vibrational spectroscopy. These studies have suggested that a variety of unusual structural features occur in these glasses, such as valence alternation pairs,⁷ new types of microstructures not present in crystalline analogs,⁸ and polymeric and clustered entities with a high degree of intermediate-range order.⁹ Caution needs to be exercised, however, in using such results to develop general models of glass structure, because most of these techniques are not inherently quantitative and tend to emphasize ordered environments.

A powerful technique that avoids the above-mentioned problems is solid-state NMR. While solid-state NMR is a well-established technique in the area of oxide (silicate, borate) glasses,¹⁰ the systematic exploration of nonoxide chalcogenide glasses by modern NMR techniques has only just begun.

This contribution deals with glasses in the P-Se system, which, owing to its wide glass-forming range (0–52 at. % P),^{11–15} and the stability of the glasses formed therein, can be considered an ideal model system. The compositional dependence of the glass-transition temperature T_g is highly distinct, revealing an abrupt increase above 40

at. % phosphorus. Using spectroscopic techniques, two principal models have been invoked, based (i) on a random network with perfect chemical ordering (maximization of P—Se bonds) and (ii) on P_4Se_n clusters embedded in a Se-rich matrix.^{16,17} Both models have been discounted by us on the basis of ^{31}P spin-echo NMR.¹⁸ Furthermore, fast magic-angle-spinning (MAS) experiments of glasses and model compounds have served to identify and distinguish quantitatively three- and four-coordinate P atoms.¹⁹ Both of these previous studies have established much of the necessary methodology and provided useful constraints for possible structural models for P-Se glasses.

The present study is devoted to the explicit quantitative aspects of this problem. Specifically, we will discuss how the results of these two complementary NMR experiments can be combined to elucidate the quantitative speciation of microstructures present in these glasses.

BACKGROUND

The usefulness of solid-state NMR in addressing structural and chemical questions in the solid state stems from the effect of internal interactions, which are highly characteristic of local environments and produce readily calculable perturbations of the nuclear-magnetic-resonance frequencies in the applied magnetic field. Among these internal interactions the magnetic dipole-dipole coupling is particularly significant, since it relates directly to internuclear distances d_{ij} . The strength of the dipolar coupling in magnetically nondilute systems is usually expressed in terms of the second moment M_{2d} (rad^2/s^2), which specifies the mean-square local field present at the nuclei under investigation due to the dipole-dipole interactions with the surrounding nuclei. In the present study, the homonuclear second moment characterizing the ^{31}P - ^{31}P interaction is of key interest. This quantity can be calculated from the internuclear distances d_{ij} by the Van Vleck equation.²⁰ For glasses of the present type usually a wide chemical shift dispersion (due to anisotropy and distribution effects) is present. Thus at

high fields, the spectral dispersion is much stronger than the dipolar interaction, and hence the second moment can be calculated by the expression

$$M_{2d} = \frac{4}{15} \left[\frac{\mu_0}{4\pi} \right]^2 I(I+1) \gamma^4 \hbar^2 N^{-1} \sum_{i \neq j} d_{ij}^{-6}. \quad (1)$$

Here, the prefactor ($\frac{4}{15}$) is the same as in the case of a heterodipolar interaction, because, due to the large differences in chemical shifts for neighboring P atoms, the flip-flop transition term does not contribute to the dipolar Hamiltonian characterizing the interaction. γ is the gyromagnetic ratio, I the spin quantum number, N the number of nuclei for which M_{2d} is calculated, and $(\mu_0/4\pi)^2$ converts the calculated results to international units.

The strength of such homonuclear dipolar couplings in solids can be probed selectively by measuring the height of a 90° - t_1 - 180° spin echo as a function of evolution time $2t_1$.²¹⁻²³ In cases where the strength of the dipolar coupling is small compared to the chemical shift dispersion (as it is encountered here), the system can be viewed as the sum of the pairwise interactions. In this case, the refocused magnetization $I_i(2t_1)$ (i.e., spin echo) for an individual spin i , experiencing multiple homonuclear interactions with n neighboring spins, can be written as^{22,24}

$$\frac{I_i(2t_1)}{I(0)} = \prod_{j \neq i}^n \cos(a_{ij}t_1), \quad (2)$$

where

$$a_{ij} = \frac{\gamma^2 \hbar (1 - 3 \cos^2 \theta_{ij})}{d_{ij}^3}, \quad (3)$$

with d_{ij} being the internuclear distance, and θ_{ij} being the angle between the internuclear vector and the external magnetic field.

In a glass or a powder, Eq. (3) must be averaged over all possible orientations θ . Expressions for θ can be obtained within a fixed reference axis system relative to the external magnetic field. It can be shown that θ_{ij} is related to the orientation of any reference coordinate system by

$$\theta_{ij} = \arccos[b \cos(\phi_{0r} + \beta_{ij}) + c], \quad (4a)$$

where

$$b = \frac{\cos(\theta_{0r} + \alpha_{ij}) - \cos(\theta_{0r} - \alpha_{ij})}{2} \quad (4b)$$

and

$$c = \frac{\cos(\theta_{0r} + \alpha_{ij}) + \cos(\theta_{0r} - \alpha_{ij})}{2}. \quad (4c)$$

Here θ_{0r} is the angle between the reference axis and the external magnetic field, ϕ_{0r} is the azimuthal angle of the external magnetic field in the reference axis system, α_{ij} is the angle between the internuclear vector and the primary reference axis, and β_{ij} is the azimuthal angle of the internuclear vector in the reference axis system. The powder average of Eq. (2) can be written as

$$\frac{I_1(2t_1)}{I(0)} = \int_0^\pi \int_0^{2\pi} \prod_{j \neq i}^n \cos(a_{ij}t_1) \sin\theta_{0r} d\phi_{0r} d\theta_{0r}. \quad (5)$$

Thus, Eq. (5) can be computed using Eqs. (3) and (4a)–(4c) as substitutions.

In magnetically nondilute compounds, the decay of the echo height $I(2t_1)$ can often be approximated as a Gaussian, using M_{2d} as calculated by Eq. (1),

$$\frac{I(2t_1)}{I(0)} = e[-M_{2d}(2t_1)^2/2]. \quad (6)$$

Since Eq. (5) requires substantial computational effort for explicit spin-echo decay calculations, it would be desirable to use Eq. (6) in its place. Therefore, we will investigate in the following whether and within which limits the Gaussian approximation for ³¹P homonuclear couplings in the P-Se glass system is valid.

Systems that contain spins with widely varying dipolar coupling strengths are more accurately described by a distribution of second moments. Therefore, we must write Eq. (6) as the sum of the decays of n individual spins,

$$\frac{I(2t_1)}{I(0)} = \frac{1}{n} \sum_{i=1}^n \frac{I_i(2t_1)}{I_i(0)} = \frac{1}{n} \sum_{i=1}^n e[-M_{i2d}(2t_1)^2/2]. \quad (7)$$

Using Eq. (7) spin-echo decays can be calculated from postulated glass structure models via Eq. (1), for comparison with experimental decays. In the present article, such comparisons form the basis for the development of possible structural models for P-Se glasses.

PROCEDURES

Experimental

Glass samples containing 5–50 at. % P were prepared and characterized by the procedures previously described. The spin-echo NMR experiments were carried out basically as described earlier;¹⁸ improvements over the previous experimental procedure include shortening of the 90° pulse lengths to 5–6 μ s, correction of the data for the feedthrough signal contribution due to misadjusted 180° pulses, and back-extrapolation of $I(2t_1)$ to zero time. (In most cases, these corrections did, however, not result in significant changes.) Preliminary ³¹P MAS-NMR results have been published by us;¹⁹ for this study additional samples have been investigated using identical experimental conditions as previously reported.

Simulations

Phosphorus distributions in individual glasses were simulated on a VAX computer by randomly placing phosphorus atoms over the sites of a cubic lattice. A zinc-blende structure was chosen as a convenient model for bonding of sp^3 hybridized atoms in a solid. The unit-cell dimension was chosen to be 5.189 Å. This represents our best nearest-neighbor distance estimate in the glasses of 2.25 Å. Phosphorus atoms were distributed in a cube of $7 \times 7 \times 7$ unit cells (2744 sites) according to the composition and experimental density¹⁴ of the glass in question.

Various different simulations were carried out. Phosphorus-phosphorus bonds were allowed to form either randomly or with specific restrictions, limiting the maximum number of P—P bonds per P-bonded P to one (P_{1P} units), two (P_{2P} units), or three (P_{3P} units), respectively. In all simulations, P atoms with four neighboring phosphorus atoms, a chemical impossibility, were excluded.

Second moments were then calculated for each individual phosphorus in the inner $3 \times 3 \times 3$ unit cell area using the Van Vleck equation [Eq. (1)] and all distances to other phosphorus in the entire volume. This was repeated for at least 200 separate volumes at each concentration. Based on the resultant second-moment distribution, the decay of the echo height $I(2t_1)$ was calculated as a function of $2t_1$ by the summation of the Gaussians of all the

phosphorus with calculated second moments, using Eq. (7). To test the validity of the Gaussian approximation, rigorous calculations, using Eq. (5) were carried out for selected cases. To reduce computation time, the distances considered here were limited to 10 Å.

Throughout all the simulations, the percentage of phosphorus with at least one nearest-neighbor phosphorus (representing P—P bonding) was strictly controlled, and was varied until the best possible match with the experimental echo-height decay was obtained. The echo-height decay is quite sensitive to this amount since the presence of a nearest-neighbor phosphorus has a large effect on the calculated second moments.

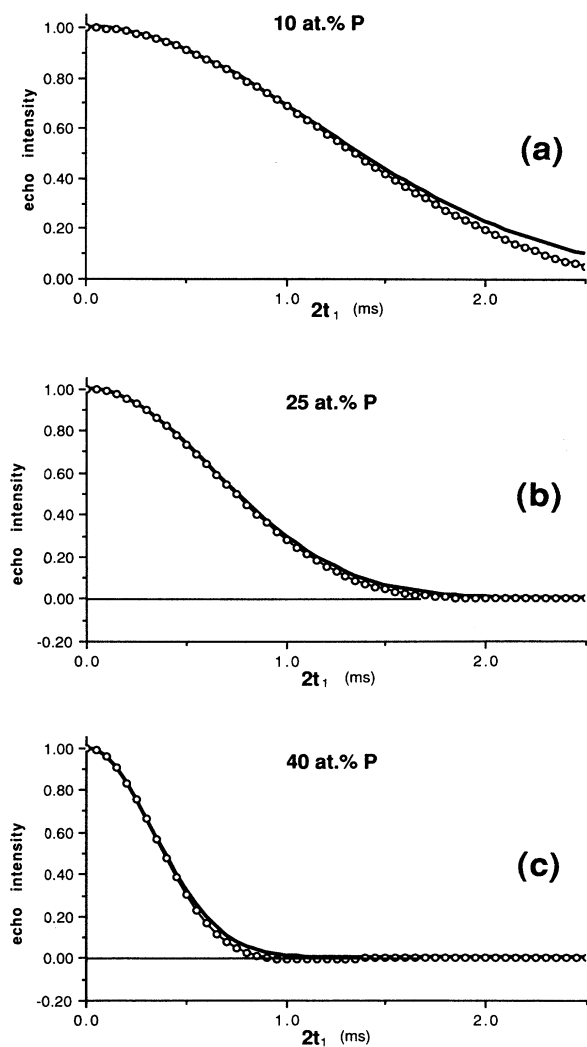


FIG. 1. Calculated spin-echo decays for representative P_{0P} units in (a) 10% P, (b) 25% P, and (c) 40% P P-Se glass simulations, showing both the rigorous calculation [Eq. (5), circles] as well as the Gaussian approximation [Eq. (6), solid line].

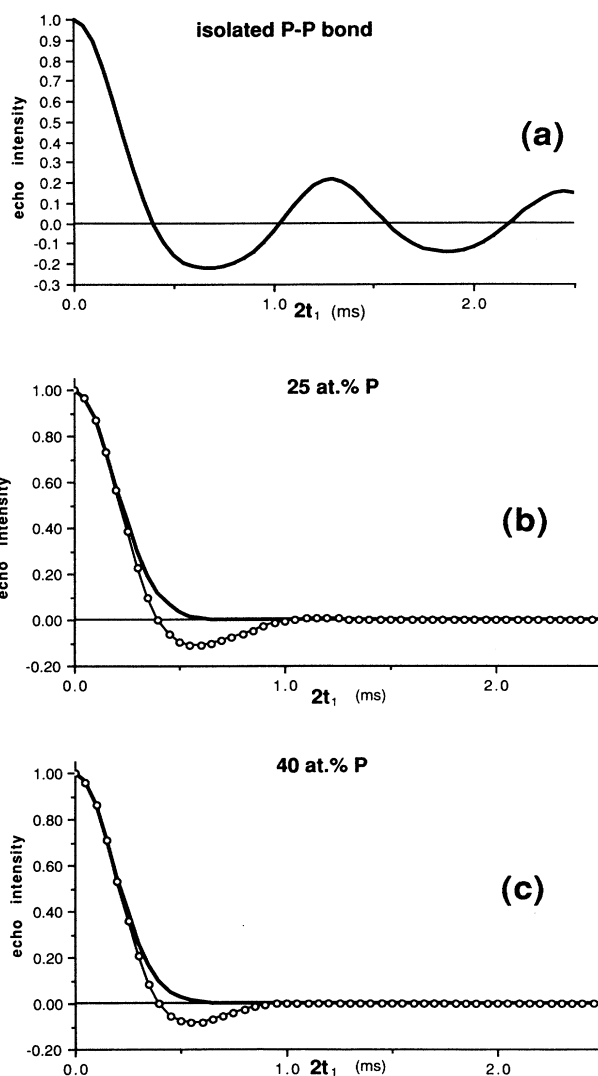


FIG. 2. Calculated spin-echo decays for representative P_{1P} units in (a) an isolated P-P unit, and in simulated glass structures containing (b) 25% P and (c) 40% P. Both the rigorous calculation [Eq. (5), circles] as well as the Gaussian approximation [Eq. (6), solid line] are shown. Note the damping of the oscillation with increasing spin density.

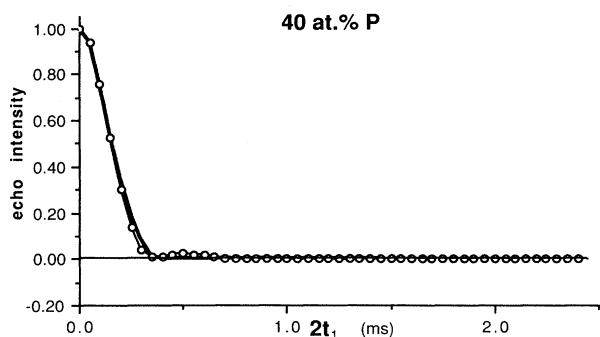


FIG. 3. Simulated spin-echo decay for representative P_{2P} units in a P-Se glass containing 40 at. % P.

RESULTS, ANALYSIS, AND INTERPRETATION

Simulations of ^{31}P spin-echo decays for distinct phosphorus species

Due to their differences in P-P internuclear interactions, the dipolar spin-echo decays of P_{0P} , P_{1P} , P_{2P} , and P_{3P} species are expected to be distinctly different, but dependent to some degree on the overall P content of the glass. This is confirmed by the results of explicit simula-

tions over the range of dipolar evolution times used in the experiment (0–2.5 ms). Figure 1 shows the calculated decay for representative P_{0P} species in (a) a glass containing 10% P, (b) a glass containing 25 at. % P, and (c) a glass containing 40 at. % P. Within the range of evolution times studied here, these decays are well-approximated by Gaussian functions.

Figure 2(a) shows the calculated decay for an isolated P—P bond of 2.25 Å length. The dipolar oscillation expected for an isolated two spin system is clearly visible. Figures 2(b) and 2(c) show the calculated decays for representative P_{1P} units in simulated glass structures containing 25 and 40 at. % P, respectively. In both cases, the weaker interactions with next-nearest P neighbors and P atoms in more remote shells have damped the oscillation arising from the two-spin system, albeit not completely removed it. The damping effect becomes more pronounced for glasses with higher P contents, due to the overall increase of the ^{31}P spin densities. Nevertheless, a Gaussian approximation of these decays would produce clear deviations within the range $0.3 \text{ ms} \leq 2t_1 \leq 0.8 \text{ ms}$.

P_{2P} and P_{3P} species have an even more rapid decay, and generally less-pronounced oscillations. The corresponding simulation for a P_{2P} species in a 40% P glass is shown in Fig. 3. Here, due to the absence of a single dominant interaction, the Gaussian approximation results in better agreement with the rigorous calculation.

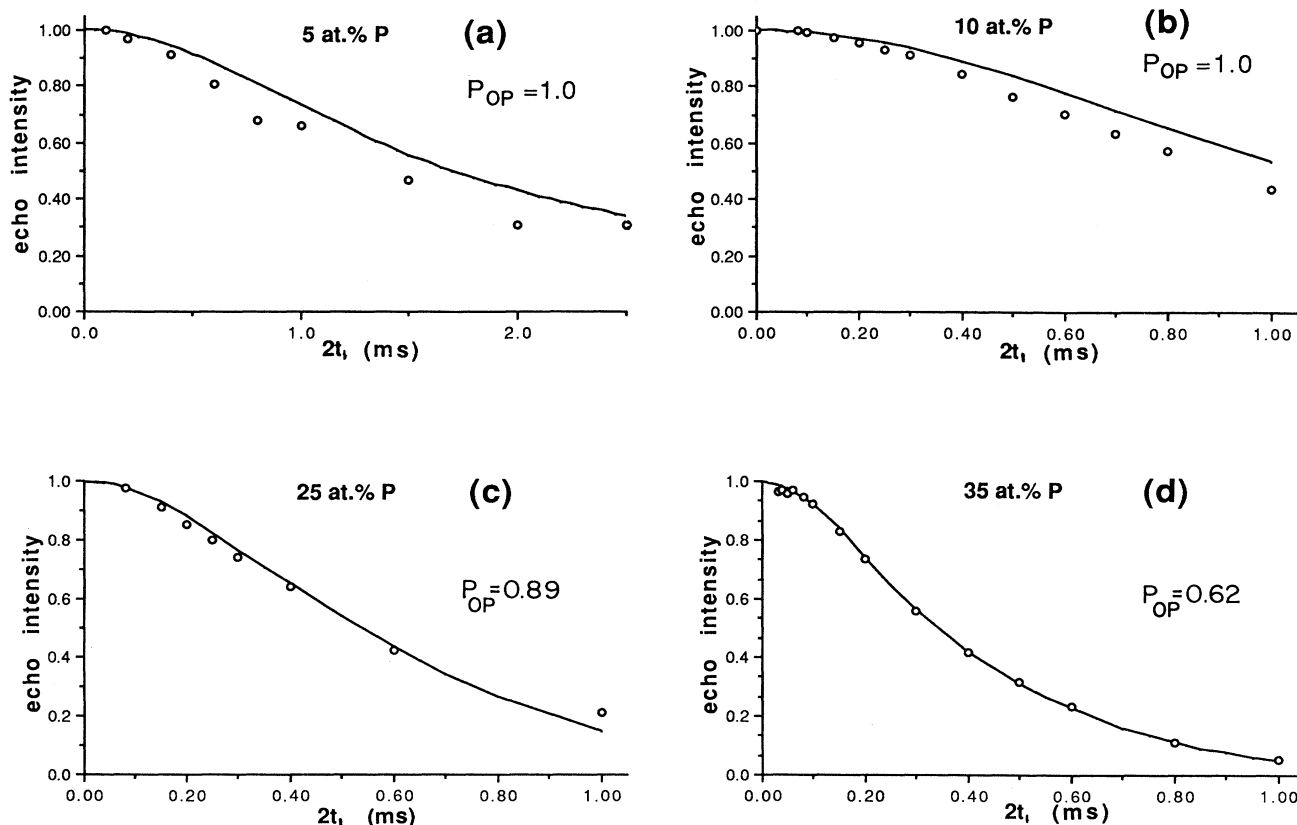


FIG. 4. Experimental spin-echo decays for some P-Se glasses (circles) compared to simulated decays (solid line) using P_{0P} fractions (P_{0P} /total P) shown. The P_{0P} fraction which best matched the experimental decay is indicated. (a) 5; (b) 10; (c) 25; and (d) 35 at. % P. Simulations (a) and (b) assume $P_{0P} = 1.0$.

Analysis of the experimental spin-echo decays

Figure 4 shows experimental spin-echo decay data for representative glasses, together with corresponding simulations, using Eq. (7). At low P contents, (5–15 at. % P), the results are consistent with a structure comprised of only P_{OP} species and excess selenium. However, simulations assuming a random distribution of P_{OP} units differ slightly, but significantly, from the experimental spin-echo decays in a consistent manner. These deviations can be attributed to two causes, both of which may be operative.

(i) First, the second-nearest-neighbor P-P distances may be closer than the value of 3.66 Å used in the present zinc-blende model. Specifically, the P-Se-P bond angle of 109.5°, implicitly assumed in connection with the zinc-blende model, is most likely too large. Taking a more realistic bond angle of 100° would reduce the second-nearest-neighbor P-P distance to 3.45 Å, hence resulting in a stronger dipolar coupling as observed.

(ii) Second, the number of second-nearest-neighbor P-P distances may be higher than expected from statistical arguments. This possibility is supported by recent ^{31}P - ^{77}Se spin-echo double-resonance (SEDOR) results obtained on this system.²⁵

The ^{31}P spin-echo decay data of glasses with 20 at. % P or more can only be fitted by assuming P-bonded phosphorus atoms in addition to P_{OP} species. However, none of the glasses studied show any indication of dipolar oscillations, suggesting that a distribution of P_{nP} species is present at any composition. The spin-echo decay is then the superposition of the various contributions shown in Figs. 1–3.

Figure 4 shows that, due to this distribution effect, it is

actually possible to simulate the experimental data artificially, by approximating the spin-echo decay of each individual P_{nP} species by Gaussians. While this approximation is an excellent one for the P_{OP} and P_{2P} units (Figs. 1 and 3), it is clearly not accurate enough for P_{1P} species (see Fig. 2). Thus in spite of the good agreement between experiment and simulations, it would be inappropriate to extract species concentrations from these fits. It is apparent, however, that the P_{OP} species completely dominate the long-term behavior of the spin-echo decay (for $2t_1 > 0.6$ ms) and there is little remaining echo intensity for any P—P bonded species beyond this point. Simulations were run with wide variations in the extent of P—P bonding while keeping the fraction of P_{OP} units constant. Little difference was seen in these simulations after $2t_1 = 0.6$ ms. It is therefore possible to obtain the number of P_{OP} units by fitting the spin-echo intensities in this range of evolution times. Thus, the experiment yields definite information about the fraction $[P_{OP}]$ of P atoms not involved in P—P bonds. This number includes both $\text{PSe}_{3/2}$ and $\text{Se}=\text{PSe}_{3/2}$ units (see below).

The remaining P atoms are involved in P—P bonding, and hence contribute only to the decay at earlier times. It would be of interest to know how many of these are P_{1P} , P_{2P} , and P_{3P} species. In principle, this information should be contained in the slope of the decay at very early evolution times ($2t_1 < 0.3$ ms). Shown in Fig. 5 is the comparison of the experimental data for a glass containing 45% P with random simulations carried out for this composition with the following built-in restrictions: (a) only P_{OP} and P_{1P} units are allowed, (b) only P_{OP} , P_{1P} , and P_{2P} units are allowed, and (c) P_{OP} , P_{1P} , P_{2P} , and P_{3P} units are allowed. Case (a) corresponds to one P—P bond for

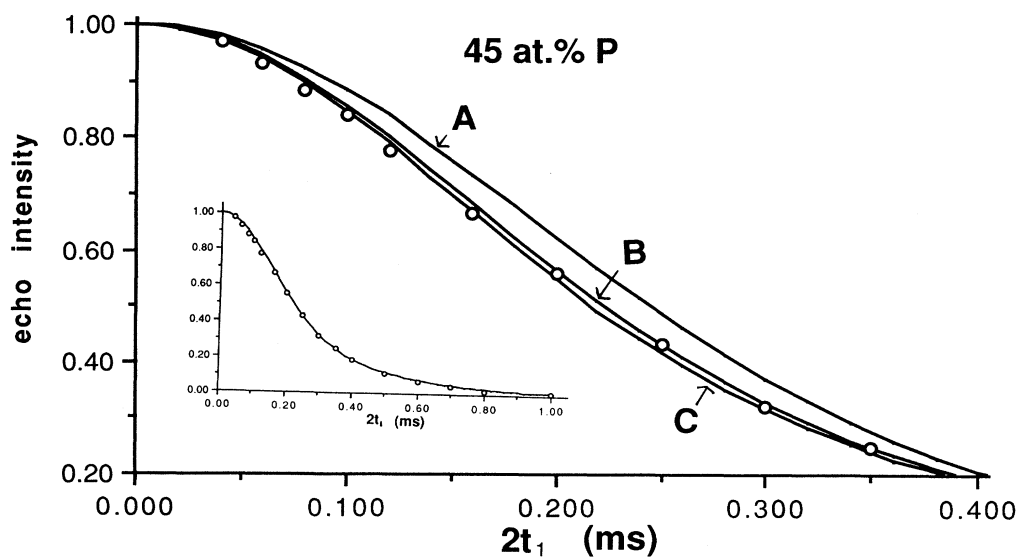


FIG. 5. Comparison of the initial experimental decay for the 45% P P-Se glass (circles) with three simulations, all with $P_{OP}=0.24$, but with differing P_{nP} distributions. A, Simulation allowing only P_{1P} and P_{OP} units. This means only one P—P bond exists for every pair of P-bonded phosphorus. B, Simulation including P_{OP} , P_{1P} , and P_{2P} species. C, Simulation including P_{OP} , P_{1P} , P_{2P} , and P_{3P} species. The inset shows the experimental data over the entire range of evolution times, together with simulation B.

every two P-bonded phosphorus atoms, whereas in the second and third cases this ratio has increased to 1.40 and 1.53, respectively. The corresponding second-moment distributions are shown in Fig. 6. Allowing P_{2P} and P_{3P} units in the random simulation clearly results in a more rapid initial decay in Fig. 5, in better agreement with the experimental data. There is only a slight difference between cases (b) and (c) because the probability of a P_{3P} species being generated in a random simulation is rather low, and hence these species do not contribute much to the overall spin-echo decay. The three simulations converge at longer evolution times, and have thus no influence on the value of $[P_{OP}]$ determined by experiment. The occurrence of P_{3P} species is questionable, as there is no precedent for such a connectivity in phosphorus chalcogenide chemistry. Table I lists the quantity $\langle n_p \rangle$, the average number of P—P bonds per P-bonded P atom, allowing P_{1P} and P_{2P} species only, for all glass compositions studied.

To summarize, the ^{31}P spin-echo experiments yield the fractions of P atoms that are involved in P—P bonds and of those that are not. Most likely, species with more than one P—P bond per P-bonded phosphorus contribute, although it is presently impossible to quantify the fractions

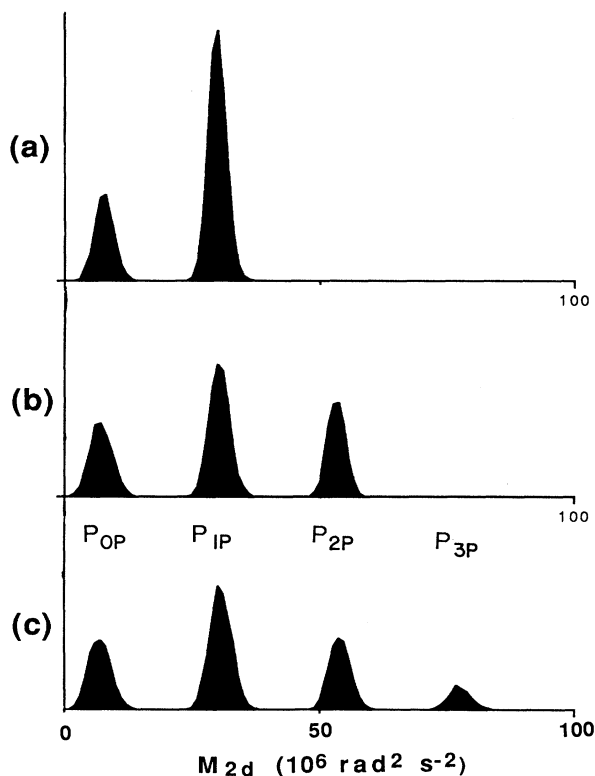


FIG. 6. The occurrence distribution of phosphorus with particular individual second moments for the three simulations shown in Fig. 5: (a) only P_{OP} and P_{1P} units are allowed; (b) P_{OP} , P_{1P} , and P_{2P} species are allowed; and (c) all P_{nP} species are allowed. The various P_{nP} species are indicated. In all simulations the P_{OP} fraction equals 0.24.

of P_{1P} , P_{2P} , and P_{3P} species from the data. The presence of such species will lead to a more Gaussian-shaped spin-echo decay, hence providing further justification for the analysis carried out here.

MAS-NMR experiments

As previously reported,¹⁹ the MAS-NMR experiments distinguish clearly between three- and four-coordinated phosphorus atoms. Figure 7 shows a typical ^{31}P MAS-NMR spectrum of a glass containing 20 at. % P. Two major peaks are observed, whose assignments are based on comparisons with the spectra of known crystalline phosphorus selenides (see Table II). In conjunction with this information, the peak centered around 120–130 ppm is assigned to three-coordinate phosphorus species. However, the ^{31}P MAS-NMR spectra cannot state explicitly the number of P and Se substituents, since Table II reveals that both $\text{PSe}_{3/2}$ and $\text{Se}_{2/2}\text{P-PSe}_{2/2}$ species resonate in the same region. The only model compounds available with P coordinated by four Se atoms are the ternary metal phosphoroselenates. Of these, only Cu_3PSe_4 has been crystallographically characterized. For Cu_7PSe_6 and Ag_7PSe_6 four coordination of the P atoms was inferred from integration of the ^{31}P MAS-NMR satellite peaks due to $^1J(^{77}\text{Se}-^{31}\text{P})$ spin-spin coupling.²⁶ Based on the chemical shift data in Table II, the upfield resonance located near 0 ppm in the glasses is assigned to four-coordinate $\text{Se}=\text{PSe}_{3/2}$ units. Note that this particular species differs from the PSe_4^{3-} species present in the model compounds; this may explain the less-than-perfect agreement in the chemical shifts.

Based on the above assignment, the fraction N_4 of four-coordinate P atoms is easily obtained by peak integration (see Table I). It was previously shown that the compositional dependence of N_4 is consistent with an equilibrium reaction $\text{PSe}_{3/2} + \text{Se} \rightarrow \text{Se}=\text{PSe}_{3/2}$ in the melt, characterized by a phenomenological equilibrium constant K_1 of 0.85 (mole fraction)⁻¹.¹⁹

Quantitative determination of the structural units in P-Se glasses

Combining the two experimental observables $[P_{OP}]$ (from spin-echo NMR) and N_4 (from MAS-NMR), we

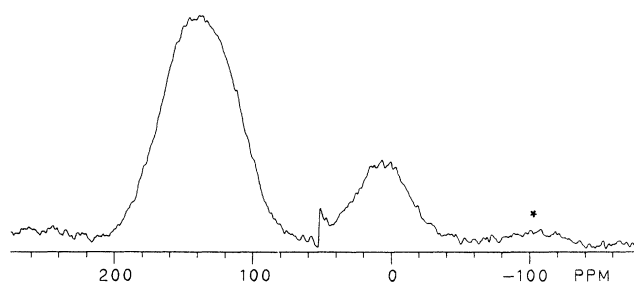


FIG. 7. ^{31}P MAS-NMR spectrum of a P-Se glass containing 20 at. % P. Spinning speed 12.6 kHz, recycle delay 10 min.

TABLE I. Species concentrations (mole fraction) and phenomenological equilibrium constants K_1 and K_2 as a function of composition in P-Se glasses.

$\{P\}^a$	$[P_{OP}]^b$	N_4^c	$\langle n_P \rangle^d$	$[PP]^e$	$[P(4)]^f$	$[P(3)]^g$	$[Se_{2/2}]^h$	K_1^i	K_2^j
0.05	1.00	0.43		0	0.022	0.029	0.854	0.91	
0.10	1.00	0.37		0	0.037	0.063	0.713	0.82	
0.125	1.00	0.33		0	0.041	0.084	0.646	0.76	
0.15	1.00	0.31		0	0.047	0.104	0.579	0.78	
0.20	0.95	0.26	1.00	0.010	0.052	0.138	0.453	0.83	
0.25	0.89	0.22	1.00	0.028	0.055	0.168	0.334	0.98	
0.30	0.78	0.15	1.12	0.066	0.045	0.189	0.242	0.98	
0.35	0.62	0.11	1.22	0.134	0.039	0.179	0.168		57.9
0.375	0.48	0.07 ^k	1.27	0.196	0.026	0.154	0.160		38.8
0.40	0.38	0.05 ^k	1.34	0.248	0.020	0.132	0.146		31.2
0.425	0.28	0.02 ^k	1.37	0.306	0.009	0.111	0.139		25.2
0.45	0.24	0.01 ^k	1.40	0.342	0.005	0.104	0.110		28.8
0.475	0.20	0.00	1.43	0.380	0.000	0.100	0.084		34.0

^aAtomic fraction of phosphorus in the glass.

^bFraction of the P atoms not involved in P—P bonds, as determined by the spin-echo experiment.

^cFraction of the P atoms tetrahedrally coordinated (present as $Se=PSe_{3/2}$ units), as determined by MAS-NMR.

^dAverage number of P bonds per P-bonded P atom, as obtained by the random simulation.

^eSpecies concentration of P-bonded P atoms (see text).

^fSpecies concentration of $Se=PSe_{3/2}$ units (see text).

^gSpecies concentration of $PSe_{3/2}$ units (see text).

^hSpecies concentration of $Se_{2/2}$ units (see text).

ⁱEquilibrium constant (mole fraction)⁻¹ characterizing the formation of $Se=PSe_{3/2}$ units, calculated for each individual composition.

^jEquilibrium constant (mole fraction)⁻¹ characterizing the homopolar vs heteropolar bond formation (see text), calculated for each individual composition.

^kEstimated values.

can now derive the detailed distribution of the particular types of structural units (as seen in Fig. 8) within the entire range of glass formation. The result of this analysis is listed in Table I and shown in Fig. 9. It is assumed that all the tetrahedrally coordinated phosphorus atoms (as determined by MAS) are not bound to other P atoms. This assumption is reasonable since little phosphorus-phosphorus bonding can be found in the compositional region where a large percentage of tetrahedral phosphorus exists. We then obtain: $[P(4)] = N_4 \{P\}$, expressed

as $Se=PSe_{3/2}$ units in Table I; $[P(3)] = ([P_{OP}] - N_4) \{P\}$, expressed as PSe_x units in Table I; $[PP] = (1 - [P_{OP}]) \{P\}$, expressed as PSe_x units, where x is given by the lever rule between the values 1, for $\langle n_P \rangle = 1$, and 0.5, for $\langle n_P \rangle = 2$. Consequently,

$$[Se_{2/2}] = 1 - 3.5[P(4)] - 2.5[P(3)] - (1+x)[PP].$$

Note again that the result obtained for the number of Se—Se bonded species depends on our assumptions on

TABLE II. ³¹P NMR chemical shifts of P-Se environments.

Unit	Compound	δ_{iso} (ppm) ^a	Ref.
$PSe_{3/2}$	α - P_4Se_3 (solid)	68,87,90	19
	β - P_4Se_3 (solid)	63	19
	P_4Se_3 (liquid)	36	27
	PAs_3Se_3 (liquid)	87	27
	β - $P_4Se_3I_2$ (liquid)	171.3	28
	P_3Se_4I (liquid)	122	29
	$P(SeC_6H_5)_3$ (liquid)	114	30
$Se_{2/2}P$ - $PSe_{2/2}$	P_4Se_4 (solid)	127	19
	α - $P_4Se_3I_2$ (solid)	110.5	19
	α - $P_4Se_3I_2$ (liquid)	105.4	28
$Se=PSe_{3/2}$	Cu_3PSe_4 (solid)	-83	26
	Cu_7PSe_6 (solid)	-28	26
	Ag_7PSe_6 (solid)	-51	26

^aValues in ppm (± 1) from H_3PO_4 .

$\langle n_p \rangle$). If it is assumed (Fig. 5 to the contrary) that each P-bonded phosphorus is involved in one and only one P—P bond (only P_{1P} allowed), the Se—Se bond unit concentration follows the solid line in Fig. 9. This curve represents the minimum Se—Se bond concentration at each composition. A better estimate for the Se—Se bond concentration can be seen as the dotted line in Fig. 9, which is based on a statistical distribution of P_{nP} species, admitting P_{1P} , P_{2P} , and P_{3P} units. This latter estimate is supported by the data in Fig. 5 and others not shown.

Note that no species concentrations are given for glasses with phosphorus content higher than 47.5 at. % MAS-NMR studies have shown that such glasses contain a considerable number of discrete P_4Se_3 molecules.¹⁹ While the fractions of these P_4Se_3 units are easily accessible from the MAS peak integrations, the orientational mobility of these units affects the spin-echo intensities, and hence renders the analysis less reliable in this compositional region. For this reason, a complete analysis has been omitted for these glasses.

DISCUSSION AND CONCLUSIONS

The results of the present study confirm our previous interpretation that the chemically ordered network model and the cluster models invoked in earlier studies are not realistic. For example, consider the cluster model, as proposed for a glass containing 25 at. % P. If the glass were composed primarily of P_4Se_5 clusters linked by selenium chains, the NMR study should reveal a 25% fraction of P_{0P} units and a 75% fraction of P_{nP} units with $n > 0$. We, however, see an 89% fraction of P_{0P} units and only an 11% fraction of P-P coordinated P units at 25 at. % P. Only when the stoichiometry of the glass approaches that of the P_4Se_5 cluster (44.44 at. % P), do our

results agree with the P_4Se_5 calculation. This is not to say that these clusters do not exist in the glasses at lower compositions, but rather that the existence of them is a consequence of the natural random distribution of atoms within the glass. It may be the case that these clusters, when they exist, are emphasized by the diffraction methods.

The host of our NMR studies points to a much more probabilistic picture of phosphorus-selenium glasses, involving a variety of structural environments all of which are present to certain amounts at a given composition. This conclusion is conceptually consistent with the model of broken chemical order previously suggested for the Ge-Se-Sn system.⁸ In spite of this general result, the NMR data also give positive evidence for subtle ordering phenomena in these glasses. There is a definite preference in the formation of P—Se over P—P bonds. This preference can again be expressed in terms of a phenomenological equilibrium constant $K_2 = [P-Se]^2/[P-P][Se-Se]$. Here $[P-Se]$, $[P-P]$, and $[Se-Se]$ denote actual bond occurrences, which can be computed for each composition from the experimental species concentrations. In calculating K_2 , we take into consideration that there are three P—Se bonds per $PSe_{3/2}$ species and $3 - \langle n_p \rangle$ P—Se bonds per P—P bonded species (the presence of terminal Se atoms has been neglected in this case). At higher P concentrations, where appreciable concentrations of P—P bonded species exist (above 30 at. % P), K_2 assumes fairly stable values. As expressed by the large value of K_2 , P—P bonds definitely occur at a sub-statistical level, and below 20 at. % P no P—P bonds are detectable within experimental error. Likewise, Se—P bonds are greatly favored over Se—Se bonds, although the latter can be found over the entire glassforming region.

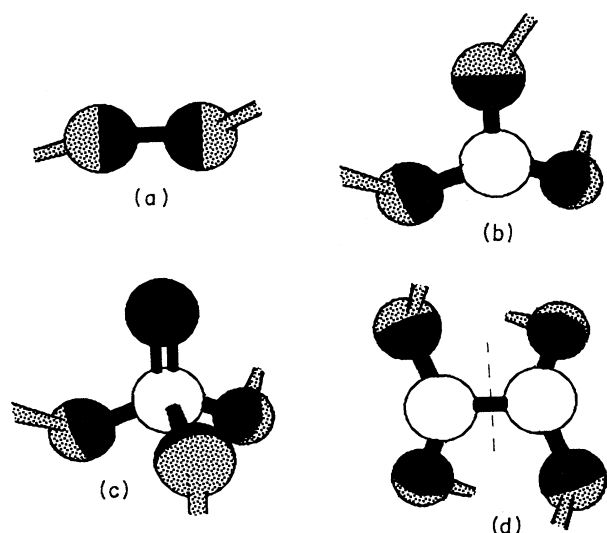


FIG. 8. Microstructural units present in P-Se glasses that have been quantitatively determined in the present study: (a) $Se_{2/2}$ units, (b) $PSe_{3/2}$ units; (c) $Se=PS_{3/2}$ units; (d) $P_2Se_{4/2}$ units.

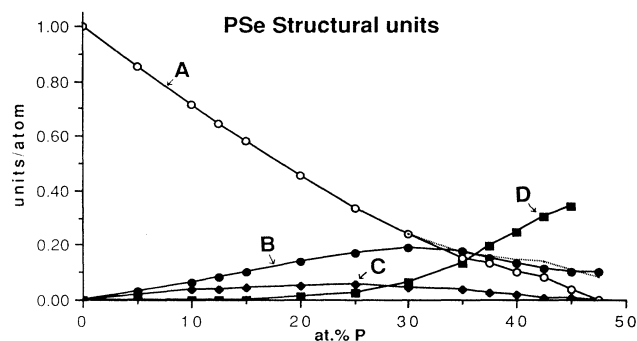


FIG. 9. The quantification of the structural units in Figs. 8(a)–8(d) as determined from the NMR data. Quantification of $Se=PS_{3/2}$ units is obtained from the ^{31}P MAS data, while the quantification of $PSe_{3/2}$ and $PSe_{2/2}$ units is from the ^{31}P spin-echo experiments. Any excess selenium is assumed to form $Se_{2/2}$ units. The solid $Se_{2/2}$ line assumes only P_{0P} and P_{1P} units exist, while the dotted line assumes that P—P bonding exists to the extent of the simulations with P_{2P} and P_{3P} units allowed as well.

While there exists a distinct driving force for the formation of $\text{PSe}_{3/2}$ groups, the reaction of these groups with excess Se to form $\text{Se}=\text{PSe}_{3/2}$ groups is much less favored. This is indicated by the near-unity value of the corresponding equilibrium constant K_1 . The multitude of structural units present at each composition tends to disfavor nucleation processes that would eventually lead to crystallization. This "chemical disorder" qualitatively explains the high tendency for glass formation in the phosphorus-selenium system and the great resistance of these glasses to recrystallization.

It is interesting to explore the relationship of the microstructural speciation shown in Fig. 9 with the compositional dependence of T_g . Inspection of Fig. 9 shows no dramatic microstructural changes or other unusual features in this compositional range. Most likely, the T_g increase is related to a depletion of longer Se_n chain units, hence restricting the possibilities of conformational mobility in these glasses. In contrast, the presence of highly mobile P_4Se_3 molecules embedded in the glass matrix appears to be unrelated to the glass transition.

In analogy with the previous discussion of the Ge-As-Se system⁶ the increase of T_g at high P concentrations (above 40 at. % P) can be rationalized on the basis of the percolation model.^{6,31} According to this model, the num-

ber of zero-frequency modes (taken as a measure of the deformability of a network) can be computed from the average valence $\langle r \rangle = \sum r_i X_{r_i}$. Here r_i and X_{r_i} are the valencies and the atomic fractions of the individual glass constituents. At the percolation threshold $\langle r \rangle = 2.4$, the number of zero-frequency modes goes to zero, resulting in an abrupt rigidification of the network structure. Application of this concept to the P-Se system reveals indeed that the composition of 40 at. % P corresponds to the rigidity percolation threshold. By establishing that the T_g change around 40 at. % P is not accompanied by or due to dramatic changes in the site speciation, the NMR studies thus lend important support to this percolation model in the conceptual description of chalcogenide glasses.

ACKNOWLEDGMENTS

This research was supported by the National Science Foundation, Grant No. DMR 89-13738 and the University of California at Santa Barbara Academic Senate. Acknowledgment is made to the Donors of the Petroleum Research Fund, administered by the American Chemical Society, for partial funding of this project.

-
- ¹P. C. Taylor, *Mater. Res. Soc. Bull.* **36** (1987).
²A. M. Andriesh, *J. Noncryst. Solids* **77/78**, 1219 (1985).
³J. H. Kennedy, *Mater. Chem. Phys.* **23**, 29 (1989).
⁴J. C. Phillips, *J. Noncryst. Solids* **34**, 153 (1979); M. F. Thorpe, *ibid.* **57**, 355 (1983).
⁵J. Z. Liu and P. C. Taylor, *Solid State Commun.* **70**, 81 (1989).
⁶M. Tatsumisago, B. L. Halfpap, J. L. Green, S. M. Lindsay, and C. A. Angell, *Phys. Rev. Lett.* **64**, 1549 (1990).
⁷S. A. Dembovskii, and E. A. Chechetkina *J. Noncryst. Solids* **85**, 364 (1986).
⁸P. Boolchand, *Hyperfine Interact.* **27**, 3 (1986).
⁹M. Tenhover, M. A. Hazle, and R. K. Grasselli, *Phys. Rev. Lett.* **51**, 404 (1983).
¹⁰G. L. Turner, R. J. Kirkpatrick, S. H. Risbud, and E. Oldfield, *Am. Ceram. Soc. Bull.* **66**, 656 (1987).
¹¹Z. U. Borisova, B. E. Kasatkin, and E. I. Kim, *Izv. Akad. Nauk SSSR Neorg. Mater.* **9**, 822 (1973) [*Inorg. Mater. (USSR)* **9**, 735 (1973)].
¹²R. Blachnik and A. Hoppe, *J. Noncryst. Solids* **34**, 191 (1979).
¹³F. Heyder and D. Linke, *Z. Chem.* **13**, 480 (1973).
¹⁴Z. U. Borisova, in *Glassy Semiconductors* (Plenum, New York, 1981), pp. 70ff.
¹⁵Y. Monteil and H. Vincent, *Z. Anorg. Allg. Chem.* **416**, 181 (1975).
¹⁶D. L. Price, M. Misawa, S. Susman, T. I. Morrison, G. K. Shenoy, and M. Grimsditch, *J. Noncryst. Solids* **66**, 443 (1984).
¹⁷M. Arai, R. W. Johnson, D. L. Price, S. Susman, M. Gay, and J. E. Enderby, *J. Noncryst. Solids* **83**, 80 (1986).
¹⁸D. Lathrop and H. Eckert, *J. Am. Chem. Soc.* **111**, 3536 (1989).
¹⁹D. Lathrop and H. Eckert, *J. Phys. Chem.* **93**, 7895 (1989).
²⁰J. H. Van Vleck, *Phys. Rev.* **74**, 1168 (1948).
²¹M. Engelsberg and R. E. Norberg, *Phys. Rev. B* **5**, 3395 (1972).
²²T. M. Duncan, D. C. Douglass, R. Csencsits, and K. L. Walker, *J. Appl. Phys.* **60**, 130 (1986); D. C. Douglass, T. M. Duncan, K. L. Walker, and R. Csencsits, *ibid.* **58**, 197 (1985).
²³P. F. Molitor, R. K. Shoemaker, and T. M. Apple, *J. Phys. Chem.* **93**, 2891 (1989).
²⁴A. Abragam, *The Principles of Nuclear Magnetism* (Clarendon, Oxford, 1964).
²⁵D. Lathrop and H. Eckert, *J. Am. Chem. Soc.* **112**, 9017 (1990).
²⁶D. Lathrop, M. Tullius, T. Tepe, and H. Eckert (unpublished).
²⁷R. Blachnik, U. Wickel, and P. Schmitt, *Z. Naturforsch. Teil B* **39**, 1135 (1984).
²⁸R. Blachnik, G. Kurz, and U. Wickel, *Z. Naturforsch. Teil B* **39**, 778 (1984).
²⁹R. Blachnik, W. Buchmeier, C. Schneider, and U. Wickel, *Z. Naturforsch. B* **42**, 47 (1987).
³⁰R. K. Shiba, N. L. Keder, and H. Eckert (unpublished).
³¹M. F. Thorpe, *J. Noncryst. Solids* **76**, 109 (1985).